Journal of Integrative Agriculture 2020, 19(1): 277–290

Available online at www.sciencedirect.com

ScienceDirect

RESEARCH ARTICLE

Soil temperature estimation at different depths, using remotely-sensed data

HUANG Ran[1], HUANG Jian-xi[1], ZHANG Chao[1], MA Hong-yuan[1], ZHUO Wen[1], CHEN Ying-yi[2], ZHU De-hai[1], Qingling WU[3], Lamin R. MANSARAY[4]

[1] *College of Land Science and Technology, China Agricultural University/Key Laboratory of Remote Sensing for Agri-hazards, Ministry of Agriculture and Rural Affairs/Key Laboratory for Agricultural Land Quality, Ministry of Natural Resources, Beijing 100083, P.R.China*

[2] *College of Information & Electrical Engineering, China Agricultural University, Beijing 100083, P.R.China*

[3] *Department of Geography, University College London, London WC1E 6BT, UK*

[4] *Department of Agro-meteorology and Geo-informatics, Magbosi Land, Water and Environment Research Centre (MLWERC), Sierra Leone Agricultural Research Institute (SLARI), Freetown PMB 1313, Sierra Leone*

Abstract

Soil temperatures at different depths down the soil profile are important agro-meteorological indicators which are necessary for ecological modeling and precision agricultural activities. In this paper, using time series of soil temperature (ST) measured at different depths (0, 5, 10, 20, and 40 cm) at agro-meteorological stations in northern China as reference data, ST was estimated from land surface temperature (LST) and normalized difference vegetation index (NDVI) derived from AQUA/TERRA MODIS data, and solar declination (Ds) in univariate and multivariate linear regression models. Results showed that when daytime LST is used as predictor, the coefficient of determination (R^2) values decrease from the 0 cm layer to the 40 cm layer. Additionally, with the use of nighttime LST as predictor, the R^2 values were relatively higher at 5, 10 and 15 cm depths than those at 0, 20 and 40 cm depths. It is further observed that the multiple linear regression models for soil temperature estimation outperform the univariate linear regression models based on the root mean squared errors (RMSEs) and R^2. These results have demonstrated the potential of MODIS data in tandem with the Ds parameter for soil temperature estimation at the upper layers of the soil profile where plant roots grow in. To the best of our knowledge, this is the first attempt at the synergistic use of LST, NDVI and Ds for soil temperature estimation at different depths of the upper layers of the soil profile, representing a significant contribution to soil remote sensing.

Keywords: soil temperature, land surface temperature, normalized difference vegetation index, solar declination

1. Introduction

Soil is an essential resource for material circulation and energy exchange between living things and the environment, and is vital in the regulation of ecosystem services (Fangueiro *et al.* 2018). Soil temperature is one of the most important components of the Earth's surface

Received 26 September, 2018 Accepted 18 February, 2019
Correspondence HUANG Jian-xi, E-mail: jxhuang@cau.edu.cn

doi: 10.1016/S2095-3119(19)62657-2

energy budget and plays an important role in climatology, agriculture, ecosystems, hydrology, and the environment.

Estimating soil temperature is useful for understanding the energy exchange between atmosphere and land (Hillel *et al.* 1998; Hu and Feng 2003; Gao *et al.* 2011) and providing valuable information on the biophysical and biochemical processes in soils. Temperature strongly influences the soil freeze and thaw states (Shati *et al.* 2018), seed sowing dates (Araghi*et al.* 2017), crop growth (Beck *et al.* 2010; Huang *et al*. 2019a) and development (Huang *et al.* 2012, 2016, 2018, 2019b; Huang R *et al.* 2015), yield (Hillel *et al.* 1998), and the rate of plant diseases and insect pests. In addition, it also influences infiltration (Jebamalar*et al.* 2012), evapotranspiration (Moran *et al.* 2009) and hence, soil water content (Tabbagh*et al.* 2016). Moreover, the crop root systems are strongly influenced by soil temperature. Generally speaking, soil temperature has greater effects on crop growth and yield than ambient air temperature in many cases (Hillel *et al.* 1998). Therefore, it is necessary to develop robust models that would estimate daily soil temperature seamlessly down the soil profile.

Most soil temperature observations across the globe are still based on *in-situ* measurements obtained at meteorological stations. Though these platforms can provide a long time series of accurate soil temperature readings at predetermined depths down the soil profile, being point-based and sparsely located across landscapes, limit their ability to truly represent the spatial dynamics of soil temperature. In this regard, several methodologies involving statistical models, interpolation techniques and remote sensing have been developed and implemented for spatio-temporal soil temperature estimation in support of ecological modeling and agronomic activities.

Univariate and multiple regression-based models have been developed to estimate soil temperature by considering various atmospheric variables, soil formation factors, terrain attributes, and location (Yang *et al.* 1989; Zhang *et al.* 1993; Barringer *et al.* 1997; Feng and Dai 2004; Mackiewicz *et al.* 2012). Yang (1989) estimated soil temperature at 50 cm depth using soil temperatures at 40 and 80 cm depths, air temperature, precipitation, and wind speed measured at eight meteorological stations from 1950 to 1980 (Yang *et al.* 1989). Barringer (1997) found a strikingly stable relationship between temperature and altitude in South Island High Country of New Zealand by multiple linear regressions between site attribute data and soil temperature data (Barringer *et al.* 1997). Mackiewicz *et al.* (2012) employed dummy predictor variables in a multiple linear regression to quantify soil temperature responses to air temperature and snow cover. Nevertheless, the spatial variability of soil temperature is modified by terrain attributes especially in heterogeneous terrain and land cover (Kang *et al.* 2000; Daly *et al.* 2006; Mackiewicz 2012; Lehnert *et al.* 2013). Lehnert *et al.* (2013) identified the geo-factors influencing soil temperature regime in Olomouc, eastern Czech Republic, and concluded that variability of the soil temperature regime was due to the physical and chemical properties of soils, topography, and atmospheric inversions.

Geo-statistics, such as kriging, inverse distance weighting, triangular irregular network, trend surface analysis, smoothing splines, and neighborhood-based functions, have been used for spatial interpolation of soil temperature on the basis of measured data (Burrough *et al.* 1986; Webster and Oliver 1992; Mitasova and Mitas 2001; Jin and Mullens 2014). And for the complex topographical region or for the purpose of modeling dynamic soil properties especially over complex topographies, more advanced interpolation algorithms were introduced using a large number of variables, including terrain attributes, spatial coordinates, and expert knowledge (Burrough 1986; Agnew and Palutikof 2000; Gasch *et al.* 2015). By comparing different mathematical interpolation methods, Wu *et al.* (2016) concluded that the interpolation method considering the effects of elevation is more accurate than others, and that the thin plate spline with latitude, longitude, and elevation, recorded the best performance in a complex topographical region. However, studies have shown that the performance of interpolation methods depends on the available independent and auxiliary datasets as well as the characteristics of the areas under study (Vicente-Serrano *et al.* 2003; Wu *et al.* 2013, 2016).

Land surface temperature (LST) retrieved from satellite images has already been used in the estimation of daily maximum air temperature (Lin *et al.* 2012; Cai *et al.* 2017; Yoo and Im 2017), minimum air temperature (Peon *et al.* 2014; Bustos and Meza 2015; Didari *et al.* 2017) and mean air temperature (Huang J X *et al.* 2015; Zhang *et al.* 2016; Wang *et al.* 2017). It has also been used to model the surface urban heat island (SUHI) effect in urbanized regions (Huang *et al.* 2017; Gaur *et al.* 2018; Meng *et al.* 2018). Besides, LST can affect soil moisture (SM), and there are several approaches that use LST to estimate SM (Song *et al.* 2014; Colliander *et al.* 2017) or monitor drought based on the temperature vegetation dryness index (TVDI) (Gao *et al.* 2011; Du *et al.* 2017; Zhang *et al.* 2017). Moreover, satellite-derived normalized difference vegetation index (NDVI) is a crucial source of information and one of the most frequently adopted vegetation indices for a variety of land applications. For example, NDVI data have been used for large-area crop mapping (Peng *et al.* 2011; Skakun *et al.* 2017), classification (Zhang *et al.* 2017), and change detection (Tong *et al.* 2017). Time series of NDVI are generally used for the assessment and monitoring of crops, forests, and grasslands (Liao *et al.* 2017), and to

estimate gross primary productivity and crop yield (Huang *et al.* 2014).

Although LST and NDVI data have been widely used in air temperature estimation, little attention has been paid to soil temperature estimation with LST data, and it has been suggested that temperatures at the upper layers of the soil profile may be a better surrogate than the near-surface air temperature for crop growth modelling and yield estimation (Shati *et al.* 2018).

Kang *et al.* (2000) reported that soil temperature is sensitive to leaf area index (LAI) in forested areas and Huang *et al.* (2008) assimilated LST and LAI into the Common Land Model (CLM) to improve the estimation of soil temperature. Soil temperature is not only related to the air temperature but also is influenced by deep soil thermal conditions. With remote sensing data, models can be applied to describe the spatial heterogeneity of soil temperature within heterogeneous topography and vegetation.

As ground-based soil temperature observations are unevenly distributed and relatively sparse in spatial terms, it is imperative to develop methods that would provide spatially seamless estimates of daily soil temperature at different depths, and this can be achieved using data acquired from Earth-observation satellites. However, the estimation of soil temperatures using satellite data is challenging and no satellite-derived soil temperature data are currently available (Shati *et al.* 2018). The relationships among soil temperature, LST and vegetation indices derived from satellite data are still not adequately explored. Therefore, the current study aims at proposing a simple but accurate approach to providing spatially continuous estimation of the daily spatial dynamics of soil temperature using moderate resolution imaging spectroradiometer (MODIS), taking northern China as case study. To this end, the univariate linear regression models were developed at depths of 0, 5, 10, 20, and 40 cm using LST, NDVI, and solar declination (Ds) as predictors, respectively. Then multivariate linear regression models were developed to estimate soil temperature at the aforementioned depths using LST, NDVI, and Ds as predictor variables. At last, the performances of the soil temperature estimation models were evaluated using the coefficient of determination (R^2) and root mean square error (RMSE), based on an independent validation dataset.

2. Data and methods

2.1. Study area

This study was conducted in an agricultural region located in northern China, including Jilin Province, Liaoning Province, Heilongjiang Province and four prefecture-level administrative divisions in eastern part of Inner Mongolia (Hulunbuir, Hinggan League, Tongliao and Chifeng). The study area lies between latitude 38°N and 54°N, and longitude 115°E and 135°E and the whole area is 1.24×10^6 km^2 in size. This area is characterized by extensive plains including the Songnen Plain, Sanjiang Plain and the Liaohe River Plain. Being surrounded by the Khingan Mountains and Changbai Mountains, the elevation of this area ranges from 0 to 2 500 m.

The study area has a temperate continental climate with an average annual temperature of –2.2 to 10°C, and the minimum and maximum air temperatures are –56.3 and 55.1°C, respectively from 2003 to 2015. In general, the air temperature decreases significantly with increasing latitude. The distribution of precipitation in this area is both spatially and temporally uneven, with an annual total ranging between 171.4 and 1 611.15 mm. The western part of the study area receives much less precipitation than the eastern part, with rainfall mainly occurring from May to September in the eastern part, whereas in the western part, rainfall mainly occurs from June to August, 60% of which is recorded in July and August.

The area under study is renowned for grain crop cultivation in China. A single-season crop cultivation system is practiced in this area with the main crops being rice, maize, and soybean. The soils are mostly dark-colored, suggesting the high amount of organic matter or humus and soil fertility in this area.

2.2. Remote sensing data

The remote sensing data used in this study are LST and NDVI. LST and NDVI were retrieved from images of MODIS satellite sensor onboard National Aeronautics and Space Administration (NASA)'s AQUA and TERRA Spacecrafts. TERRA and AQUA were launched on 12 Dec. 1999 and 4 May 2002, respectively. Each satellite observes the entire Earth's surface every one to two days, and retrieves data at 36 spectral bands. The data products derived from MODIS observations are crucial for studying the change of the atmosphere (He *et al.* 2017), land (Friedl *et al.* 2002), cryosphere (Casey *et al.* 2017), and ocean (Petrou and Tian 2017). MODIS LST and NDVI products use a sinusoidal grid tiling system. Each tile covers 10 degrees by 10 degrees at the equator. Tiles used in this study are h25v03, h25v04, h26v03, h26v04, h27v04 and h27v05.

The MODIS LST products can be obtained using a generalized Split-Window algorithm (Wan *et al.* 1996) with a pair of MODIS daytime and nighttime in seven TIR bands, atmospheric temperature and water vapor. With the different

atmospheric absorptions of MODIS radiance data in bands 31 and 32, linearizing or nonlinearizing the radiative transfer equation can retrieve surface emissivity and temperature. The coefficients of this split-window algorithm were determined based on viewing angle, total column water and surface air temperature (Wan *et al.* 1996). The LSTs used in this study is the daily MODIS LST products, at 1-km spatial resolution. MOD11A1 is the TERRA MODIS LST product which can provide daytime and nighttime LST at 10:30 a.m. (LST_{TD}) and 10:30 p.m. (LST_{TN}) along with quality assessment. MYD11A1 is the AQUA MODIS LST product which can provide daytime and nighttime LST at 1:30 p.m. (LST_{AD}) and 1:30 a.m. (LST_{AN}) along with quality assessment.

NDVI data were derived from the 16-day TERRA MODIS vegetation index product at 1-km spatial resolution (MOD13A2). We collected the MOD11A1, MYD11A1 and MOD13A2 products acquired from 2003 to 2013 *via* the Land Processes Distributed Active Archive Center (LP DAAC). Vegetation indices (VIs) are different combinations of two or more spectral bands which can provide more information than a single spectral band. A lot of VIs, such as NDVI, ratio vegetation index (RVI), soil adjusted vegetation index (SAVI), atmospherically resistant vegetation index (ARVI), ratio analysis of reflectance spectra (RARS), modified soil adjusted vegetation index (MSAVI), optimized soil adjusted vegetation index (OSAVI), photochemical reflectance index (PRI), pigment specific simple ratio & pigment specific normalized difference (PSSR & PSND), aerosol free vegetation index (AFVI), and the enhanced vegetation index (EVI), have been developed for the study of vegetation. Most VIs use red, and the near infrared (NIR) spectral bands. These VIs have been proven to be good indicators of vegetation state and dynamics. The NDVI, which is one of the most widely used vegetation index, can be calculated as follows:

$$\mathrm{NDVI}=\frac{\rho_{\mathrm{NIR}}-\rho_{\mathrm{Red}}}{\rho_{\mathrm{NIR}}+\rho_{\mathrm{Red}}} \quad (1)$$

The vegetation absorbs most of the red radiation due to the pigments and reflects most of the NIR radiation due to the leaf cellular structure. In order to get daily NDVI data, the 16-day MODIS NDVI was reconstructed based on the Savitzky-Golay (S-G) filter.

2.3. *In-situ* soil temperature measurements

Soil temperature (ST) data were acquired from 2003 to 2015 at 53 meteorological stations in the study area. Soil temperatures were observed at depths of 0, 5, 10, 20, and 40 cm. Among these 53 stations, there are 15 in Liaoning Province, 13 in Jilin Province, 13 in Heilongjiang Province and 12 in the eastern part of Inner Mongolia. The 53 stations were chosen such that they cover a wide range of climatic, topographic, soil, and land cover features. We sorted these 53 stations by altitude, and selected a validation station for every three stations. The 53 stations were thus divided into two categories; calibration and validation datasets. The calibration dataset included soil temperature measurements acquired from 2003 to 2013 at 35 stations, which are Aihui, Sunwu, Bei'an, Kunshan, Hailun, Fujin, Anda, Yilan, Harbin, Boli, Haoertu, Balinzuoqi, Shebotu, Fuyu, Nong'an, Shuangliao, Shuangyang, Yongji, Jiaohe, Gangzi, Aohanqi, Zhangwu, Fuxin, Xifeng, Panshi, Helong, Yanji, Ningchengxian, Chaoyang, Shenyang, Liaoyang, Xinbin, Jianchang, Xingcheng and Dawa. Whereas the validation dataset comprises soil temperature measurements of the remaining 18 stations from 2003 to 2013, which are Jiagedaqi, Xiaoergou, Fuyu, Huerle, Bayan, Qianguo, Zhalute, Changling, Alukeerqinqi, Kailu, Wangqing, Baoguotu, Changtu, Kaiyuan, Yixian, Heishan, Linjiang and Haicheng, and data acquired from all 53 stations from 2014 to 2015.

2.4. Data processing and estimation models

The MODIS Reprojection Tool (MRT) was used to preprocess the MODIS data used in this study. We first converted the original Sinusolidal projection of daily MODIS LST products (MOD11A1 and MYD11A1) and 16-day VI products (MOD13A2) into Standard Albert projection. Then, we extracted the corresponding datasets, including LST_Day_1km, QC_Day, LST_Night_1km, and QC_Night datasets from both MYD11A1 LST products and MOD11A1 LST products, and NDVI and NDVI quality from the MOD13A2 VI product. Finally, mosaicked tiles of each dataset were produced.

Variations of NDVI can reflect the gradual process of vegetation growth. The curves of NDVI time-series are continuous and smooth as the NDVI data reflect the state and dynamics of vegetation (Chen *et al.* 2004). MODIS NDVI data in this study have a fixed and uniform interval of 16 days. They were prepared by noise reduction and smoothened to a continuous daily time-series. The method used in this study is based on the Savitzky-Golay (S-G) filter. The S-G filter is a simplified least-squares-fit convolution for smoothing consecutive data (Savitzky and Golay 1964). The general equation of the simplified least-squares convolution for NDVI time-series smoothening is given as follows:

$$\mathrm{NDVI}_{S\_G,j}=\frac{\sum_{i=-K}^{K}C_i\mathrm{NDVI}_{o,j+i}}{L} \quad (2)$$

where $\mathrm{NDVI}_{o,j+i}$ is the original NDVI value, $\mathrm{NDVI}_{S\_G,j}$ is the calculated NDVI value, K is the half-width of the smoothing

window, and $L=2K+1$. The coefficients of an S-G filter (C_i) can be given as a polynomial of certain degree. The degree of the polynomial is usually set in the range from 2 to 4. In this study, we used the second degree polynomial ($K=2$). A lower degree of the polynomial produces a smoother result but may introduce bias, and a higher degree of the polynomial may "over fit" the data. The S-G filter replaces the noise values of NDVI and preserves the upper NDVI envelope.

Solar declination (Ds), expressed in degrees is a function of the day of the year and influences the spatial distribution of solar radiation. The change in Ds throughout the year ranges from –23.442° at winter solstice to 23.442° at summer solstice, and it equals zero at the equinoxes (Bourges *et al.* 1985). It can be calculated using the eq. (3):

$$Ds=23.45\sin(360°\times\frac{284+t}{365}) \quad (3)$$

where t is the day of year, beginning from the 1st January.

The estimation models of soil temperature at different depths in northern China were developed by multiple linear regressions that describe how the target variable of interest (soil temperature) at different depths is related to LST, NDVI and Ds. The linear regression model used for soil temperature estimation is given in eq. (4):

$$ST_d=a\text{LST}+b\text{NDVI}+c\text{Ds}+\varepsilon \quad (4)$$

where ST_d is the soil temperature at depth d, d=0, 5, 10, 15, 20 and 40 cm, respectively. LST represents LST_{TD}, LST_{TN}, LST_{AD}, and LST_{AN}, respectively, a, b and c are regression coefficients, and ε is the random error. The R^2 and RMSE were used to evaluate the soil temperature estimation accuracy of the linear regressions used in this study.

3. Results

3.1. Soil temperature estimation with univariate linear regression models

A series of univariate linear regression models were built with different depths of ST as dependent variables, and with LST_{AD}, LST_{AN}, LST_{TD}, LST_{TN}, NDVI or Ds as independent variables, respectively, using calibration data from 2003 to 2013. The calibration areas were selected based on the availability of satellite-derived LSTs ($LST_{AD,}$ LST_{AN}, LST_{TD} and LST_{TN}). The R^2 and RMSEs values of these models are given in Table 1. The results show that the univariate linear regression models are significant at the 0.001 confidence level. The R^2 values range from 0.13 to 0.90 and RMSE from 2.37 to 7.15. At the same soil layer, the univariate linear regression models for soil temperature estimation using TERRA nighttime LST as estimator produced the most accurate estimates by virtue of recording the highest R^2 values and the lowest RMSE. For instance, at the 0 cm layer, using TERRA nighttime LST data as predictor of soil temperature, an R^2 of 0.83 and an RMSE of 3.79 were recorded. For Ds, the R^2 decrease from 0.77 at 0 cm to 0.52 at 40 cm with corresponding RMSE values ranging from 6.54 to 7.15. On the other hand, the R^2 between soil temperatures and NDVI increase from 0.47 at the 0 cm layer to 0.72 at the 40 cm layer. This means that the estimator of LSTs or Ds and NDVI are complementary.

Using LSTs as estimator, all R^2 values are significant at the 0.01 confidence level. The R^2 values between soil temperature and nighttime LST are higher than daytime LST for both TERRA and AQUA satellite data, and RMSEs are also smaller for models based on nighttime LSTs. For example, the R^2 values between soil surface temperature (0 cm) and daytime LST are 0.67 and 0.69, with RMSEs of 4.72 and 4.64 for AQUA and TERRA, respectively. The univariate estimation model of soil temperature at the 0 cm layer using nighttime LST as predictor recorded R^2 values of 0.79 and 0.83, with RMSEs of 3.89 and 3.79 for AQUA and TERRA, respectively. At 40 cm, the R^2 values between ST and daytime LST are only 0.13 and 0.14, with RMSEs of 5.5 and 5.58, but their R^2 values with nighttime LST are 0.66 and 0.72, with RMSEs of 4.05 and 3.72 for AQUA and TERRA, respectively. At daytime, the R^2 between soil temperature and LST decrease with soil depth rapidly with a corresponding increase in RMSE. At nighttime, the

Table 1 R^2 and RMSE for the univariate estimation models of soil temperature using land surface temperature (LST), normalized difference vegetation index (NDVI) and solar declination (Ds)[1)]

Depth (cm)	LST_{AD}		LST_{AN}		LST_{TD}		LST_{TN}		NDVI		Ds	
	R^2	RMSE	R^2	RMSE	R^2	RMSE	R^2	RMSE	R^2	RMSE	R^2	RMSE
0	0.67	4.72	0.79	3.89	0.69	4.64	0.83	3.79	0.47	6.16	0.77	7.15
5	0.52	4.8	0.83	3.02	0.55	4.75	0.9	2.55	0.47	5.17	0.74	6.54
10	0.45	4.89	0.83	2.96	0.46	4.87	0.9	2.37	0.62	4.82	0.71	6.58
15	0.37	5.01	0.81	3.04	0.38	5.01	0.9	2.45	0.64	4.67	0.68	6.69
20	0.29	5.14	0.77	3.26	0.31	5.16	0.86	2.7	0.66	4.54	0.64	6.76
40	0.13	5.5	0.66	4.05	0.14	5.58	0.72	3.72	0.72	4.35	0.52	6.76

[1)] AD, AN, TD and TN refer to AQUA daytime, AQUA nighttime, TERRA daytime, and TERRA nighttime, respectively; RMSE, root mean squared error.

R^2 between soil temperatures and LST increases first and reaches the maximum at 10 cm where the minimum RMSE is recorded. Below 10 cm depth, R^2 decreases with a corresponding increase in RMSE, indicating a progressive decline in accuracy.

3.2. Soil temperature estimation with multivariate linear regression models

Table 2 presents the multivariate linear regression models for soil temperature estimation at different depths using AQUA/TERRA daytime and nighttime LST, NDVI and Ds as predictors based on *in-situ* calibration using training stations' data from 2003 to 2013. The results show that all estimation models are significant at the 0.001 confidence level. The R^2 ranges from 0.71 to 0.92 and RMSE from 2.16 to 3.34. Compared with the results in Table 1, it can be seen that the multivariate linear regression models for the estimation of soil temperature have lower RMSEs and higher R^2 than those of the univariate linear regression models at the same soil layer. This means that the multiple linear regression models for the estimation of soil temperature outperformed the univariate linear regression models. The R^2 values decrease from the 0 cm to the 40 cm soil layers. With nighttime LSTs as predictor variables, the R^2 values are higher at the 5, 10 and 15 cm layers than those at 0, 20 and 40 cm, and soil temperature estimates with nighttime LST generally recorded higher R^2 values than corresponding estimates obtained from daytime LST.

Among the six soil depths investigated, the multivariate linear regression models constructed at the 5 cm depth produced the highest R^2. The R^2 of soil temperature estimation models decrease progressively from the 5 cm to the 40 cm layers, with estimates based on TERRA LST recording higher R^2 values at both day and night time estimation scenarios.

3.3. Validation of soil temperature estimation models

Two validations were implemented in this study: spatial and temporal. Fig. 1 presents the scatterplots of measured and estimated soil temperatures at 0, 5, 10, 20, and 40 cm based on validation data from 2003 to 2013 that correspond to AQUA and TERRA satellite overpasses (day and night), respectively. All figures show the points to be distributed along the 1:1 line, suggesting a robust estimation of soil temperatures. Table 3 shows the validation of measured and estimated soil temperatures at 0, 5, 10, 20, and 40 cm based on all *in-situ* measurements and corresponding day and night satellite (MODIS AQUA and TERRA) signals from

Table 2 Estimation models of soil temperature at different depths using land surface temperature (LST), normalized difference vegetation index (NDVI) and solar declination (Ds) as predictors using the training stations' data from 2003 to 2013[1)]

Depth (cm)	Model	R^2	RMSE	*P*-value	MAE	*n*
0	ST_0=0.624LST_{AD}+19.241NDVI+0.136Ds–7.453	0.89	2.70	0.000	2.13	14 288
	ST_0=0.744LST_{AN}+4.899NDVI+0.206Ds+9.324	0.85	3.34	0.000	2.70	17 652
	ST_0=0.673 LST_{TD}+19.539NDVI+0.111Ds–7.69	0.90	2.67	0.000	2.10	16 150
	ST_0=0.771 LST_{TN}+3.407NDVI+0.209Ds+8.704	0.86	3.24	0.000	2.60	22 679
5	ST_5=0.49LST_{AD}+21.197NDVI+0.086Ds–6.681	0.86	2.57	0.000	2.01	13 796
	ST_5=0.652LST_{AN}+8.802NDVI+0.135Ds+6.854	0.88	2.63	0.000	2.12	16 609
	ST_5=0.523LST_{TD+}21.475NDVI+0.069Ds–6.773	0.88	2.49	0.000	1.96	15 540
	ST_5=0.741LST_{TN}+5.862NDVI+0.112Ds+6.426	0.92	2.27	0.000	1.81	21 490
10	ST_{10}=0.458LST_{AD}+22.3NDVI+0.032Ds–6.53	0.85	2.63	0.000	2.06	13 799
	ST_{10}=0.626LST_{AN}+10.641NDVI+0.083Ds+6.159	0.86	2.63	0.000	2.11	16 614
	ST_{10}=0.489LST_{TD}+22.605NDVI+0.016Ds–6.621	0.86	2.54	0.000	1.99	15 544
	ST_{10}=0.729LST_{TN}+7.335NDVI+0.054Ds+5.799	0.92	2.16	0.000	1.73	21 499
15	ST_{15}=0.434LST_{AD}+23.313NDVI - 0.012Ds–6.364	0.81	2.70	0.000	2.09	13 799
	ST_{15}=0.609LST_{AN}+12.230NDVI+0.038Ds+5.619	0.86	2.67	0.000	2.13	16 613
	ST_{15}=0.464LST_{TD}+23.592NDVI - 0.027Ds–6.457	0.83	2.61	0.000	2.00	15 545
	ST_{15}=0.715LST_{TN}+8.694NDVI+0.006Ds+5.362	0.92	2.18	0.000	1.73	21 502
20	ST_{20}=0.411LST_{AD}+24.1NDVI–0.049Ds–6.242	0.79	2.81	0.000	2.16	13 791
	ST_{20}=0.5585LST_{AN}+13.746NDVI–0.001Ds+5.011	0.85	2.77	0.000	2.21	16 602
	ST_{20}=0.484LST_{TD}+24.409NDVI - 0.064Ds–6.327	0.81	2.71	0.000	2.11	15 534
	ST_{20}=0.694 LST_{TN}+10.01NDVI–0.034Ds+4.858	0.90	2.31	0.000	1.83	21 489
40	ST_{40}=0.337LST_{AD}+25.541NDVI–0.163Ds–5.679	0.71	3.17	0.000	2.41	12 766
	ST_{40}=0.529LST_{AN}+16.723NDVI–0.132Ds+3.405	0.81	3.01	0.000	2.41	15 922
	ST_{40}=0.347LST_{TD}+25.837NDVI–0.172Ds–5.535	0.74	3.12	0.000	2.39	14 517
	ST_{40}=0.608LST_{TN}+13.422NDVI–0.157Ds+3.327	0.85	2.74	0.000	2.17	20 480

[1)] AD, AN, TD and TN refer to AQUA daytime, AQUA nighttime, TERRA daytime, and TERRA nighttime, respectively; RMSE, root mean squared error; MAE, mean absolute error.

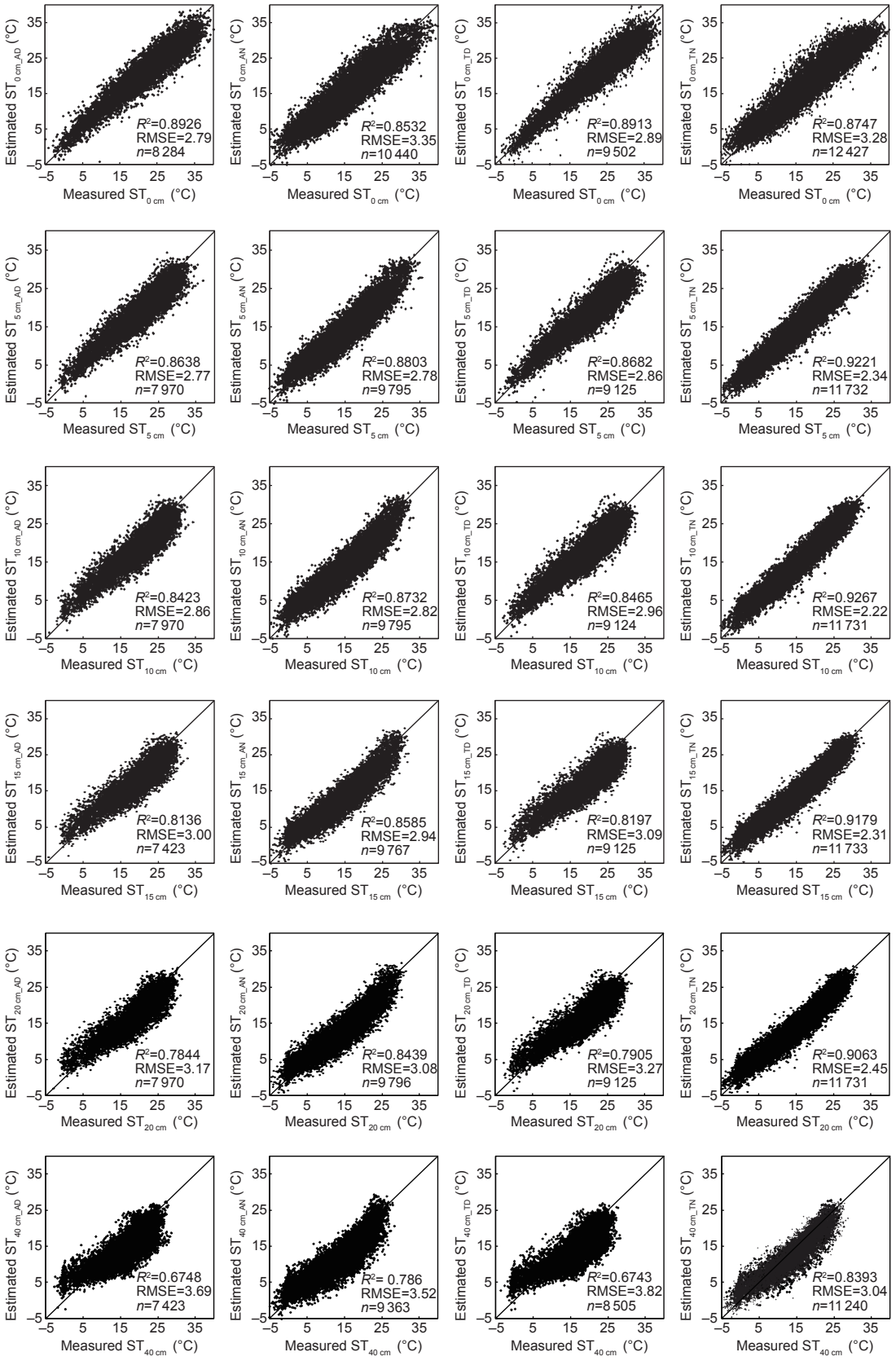

Fig. 1 Scatterplots of measured soil temperature (ST) from 18 validation stations and estimated soil temperature at the 0, 5, 10, 15, 20 and 40 cm layer from 2003 to 2013 based on remotely-sensed data. AD, AN, TD and TN refer to AQUA daytime, AQUA nighttime, TERRA daytime, and TERRA nighttime, respectively; RMSE, root mean squared error.

Table 3 Validation of measured soil temperature from 53 validation stations and estimated soil temperature from 2014 to 2015 based on remotely-sensed data[1)]

Depth (cm)	Variables	R^2	RMSE	*n*
0	LST_{TN}, NDVI, Ds	0.8516	3.40	3 299
0	LST_{AN}, NDVI, Ds	0.8449	3.30	4 577
0	LST_{TD}, NDVI, Ds	0.8717	3.17	2 560
0	LST_{AD}, NDVI, Ds	0.8765	3.10	3 887
5	LST_{TN}, NDVI, Ds	0.9136	2.37	3 298
5	LST_{AN}, NDVI, Ds	0.867	2.75	4 580
5	LST_{TD}, NDVI, Ds	0.854	3.06	2 559
5	LST_{AD}, NDVI, Ds	0.854	2.97	3 887
10	LST_{TN}, NDVI, Ds	0.9145	2.29	3 294
10	LST_{AN}, NDVI, Ds	0.8504	2.83	4 580
10	LST_{TD}, NDVI, Ds	0.8291	3.18	2 557
10	LST_{AD}, NDVI, Ds	0.825	3.11	3 884
15	LST_{TN}, NDVI, Ds	0.9077	2.36	3 294
15	LST_{AN}, NDVI, Ds	0.8338	2.94	4 580
15	LST_{TD}, NDVI, Ds	0.8081	3.32	2 553
15	LST_{AD}, NDVI, Ds	0.7962	3.25	3 881
20	LST_{TN}, NDVI, Ds	0.8894	2.55	3 298
20	LST_{AN}, NDVI, Ds	0.816	3.13	4 580
20	LST_{TD}, NDVI, Ds	0.7751	3.36	2 560
20	LST_{AD}, NDVI, Ds	0.7715	3.38	3 888
40	LST_{TN}, NDVI, Ds	0.7991	3.27	3 298
40	LST_{AN}, NDVI, Ds	0.7704	3.49	4 578
40	LST_{TD}, NDVI, Ds	0.6432	4.05	2 559
40	LST_{AD}, NDVI, Ds	0.6767	3.82	3 885

[1)] LST, land surface temperature; NDVI, normalized difference vegetation index; Ds, solar declination; TN, AN, TD and AD refer to TERRA nighttime, AQUA nighttime, TERRA daytime, and AQUA daytime, respectively; RMSE, root mean squared error.

2014 to 2015. The resultant R^2 values of two validations range from 0.67 to 0.93 and RMSEs from 2.22 to 3.69. Similar to the results of models involving training data, R^2 values decrease from the 0 cm layer to the 40 cm layer when the AQUA/TERRA daytime satellite data were used as estimators. But R^2 values attain their maximum at 5 or 10 cm when nighttime satellite data were employed as estimators of soil temperature. On the other hand, the RMSEs at 5 cm are the lowest among the different depths (0, 5, 10, 20, and 40 cm) when daytime or nighttime LSTs derived from AQUA/TERRA MODIS data are used as estimators.

4. Discussion

4.1. Mechanisms of soil temperature with remotely-sensed data

It is observed based on results obtained in this study that the differences in correlation coefficients are associated with the diurnal and seasonal variations of solar radiation. Generally, during daytime the soil surface absorbs incoming (shortwave) solar radiation which exceeds the emitted longwave (terrestrial) radiation. With the absence of insolation at night, the soil surface emits terrestrial radiation. It is observed that LST exhibits larger magnitudes when compared to soil temperature at different depths during daytime (Fig. 2). Additionally, the seasonal variation of soil temperature is a function of incident solar radiation, which dictates the LST dynamics. It is therefore apparent that the seasonal variations in deep soil temperature are much less, and lag significantly behind seasonal changes in LST. The deep soil temperatures increase more slowly with lesser fluctuations than LST in spring. In contrast, the deep soil cools more slowly than the land surface in autumn. This makes the deep soil cooler than the land (soil) surface in summer (making it a heat sink), but warmer than the land (soil) surface in winter (making it a heat source).

Based on the above account, LST, NDVI, and Ds are excellent predictors of soil temperature at different depths. The multiple linear regression models used in the current study have provided a simple but practical solution to problems encountered in the estimation of soil temperature by integrating LST and NDVI with auxiliary solar declination data. The current study revealed the potential of utilizing LST and NDVI obtained from MODIS, as well as Ds, to estimate soil temperature. Further studies are needed to validate our proposed models with related remotely-sensed data such as the Visible Infrared Imaging Radiometer Suite (VIIRS) onboard the Suomi National Polar-Orbiting Partnership (S-NPP) (Yu *et al.* 2005; Guillevic *et al.* 2012, 2014; Li *et al.* 2014; Liu *et al.* 2015; Islam *et al.* 2017; Niclòs *et al.* 2018) and Fengyun polar-orbit satellite series (Jiang *et al.* 2015; Tang *et al.* 2015; Song *et al.* 2017).

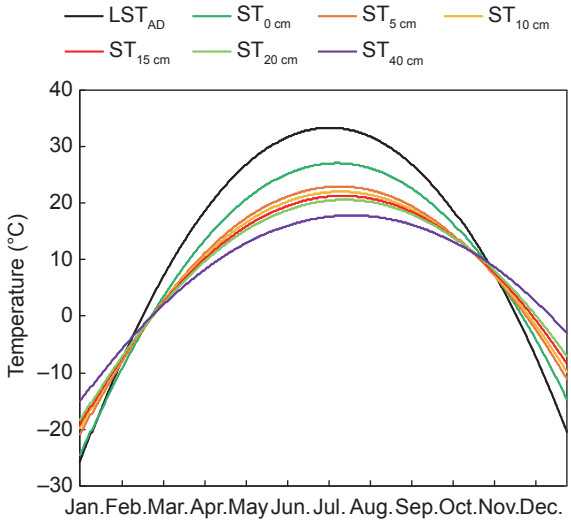

Fig. 2 Seasonal variation of land surface temperature (LST) and soil temperature (ST) at different depths from 0 to 40 cm at the Fuyu County Meteorological Station, Jilin Province, China (2015). AD, AQUA daytime.

4.2. Uncertainties in the estimation of soil temperature using remotely-sensed data

In this study, MODIS LST and NDVI data were used to estimate soil temperatures at 0, 5, 10, 20, and 40 cm. The results showed that the algorithms employed were robust in soil temperature estimation within the top 40 cm layers of the soil profile.

It is important to note that similar to all the parameter estimation models with optical satellite imagery, errors are also apparent with the soil temperature estimation algorithms proposed in the current study. Clouds have a great influence on the estimation of soil temperature because only optical images acquired under clear-sky conditions can be used for model construction. To minimize the influence of cloud cover, cloud contaminated pixels were masked out during model construction. Figs. 3 and 4 show the percentage distribution of the good quality of LST pixels from 2003 to 2015 which covers the study area, and it is observed that the good quality percentage for most pixels is below 60%. This is capable of introducing several uncertainties in the resulting soil temperature estimation. To ameliorate this potential source of uncertainty in remote sensing-based soil temperature estimation, future studies can explore data obtained from microwave satellite sensors which are capable of all-weather imaging (Fily *et al.* 2003; Gao *et al.* 2008; Chen *et al.* 2011; Yang and Weng 2011; Prigent *et al.* 2016; Zhou *et al.* 2017, 2018, 2019). LSTs and vegetation indices retrieved from microwave satellite data can eliminate the influence of clouds and their shadows, which is attendant with optical imagery like MODIS, on soil temperature estimation. Additionally, geostationary optical satellites with their high temporal resolution can increase the chance of acquiring more cloud-free images for use in soil temperature estimation (Göttsche and Olesen 2001; Sobrino and Romaguera 2004; Tang *et al.* 2008; Freitas *et al.* 2010; Rasmussen *et al.* 2011; Göttsche *et al.* 2013; Duguay-Tetzlaff *et al.* 2015; Jiang and Liu 2015; Wu *et al.* 2015; Kou *et al.* 2016; Mechri *et al.* 2016; Liu *et al.* 2017).

The second source of uncertainty in the soil temperature estimation implemented in this study is related to an *in-situ* dataset acquired from sparsely distributed meteorological stations. The spatial resolution of MODIS LST and NDVI are 1 km. Most pixels are located in areas of heterogeneous cover which exhibit different emissivity and temperature in space and time. A MODIS pixel under heterogeneous cover is a complex mixture of vegetation, bare soil, built-up, water etc., and this may complicate LST retrieval and the relationship between *in-situ* soil temperature and the LST and NDVI parameters. Additionally, precipitation changes soil water content, a parameter that also changes the soil heat capacity. The higher the soil moisture, the higher the soil heat capacity and the lesser the fluctuations of

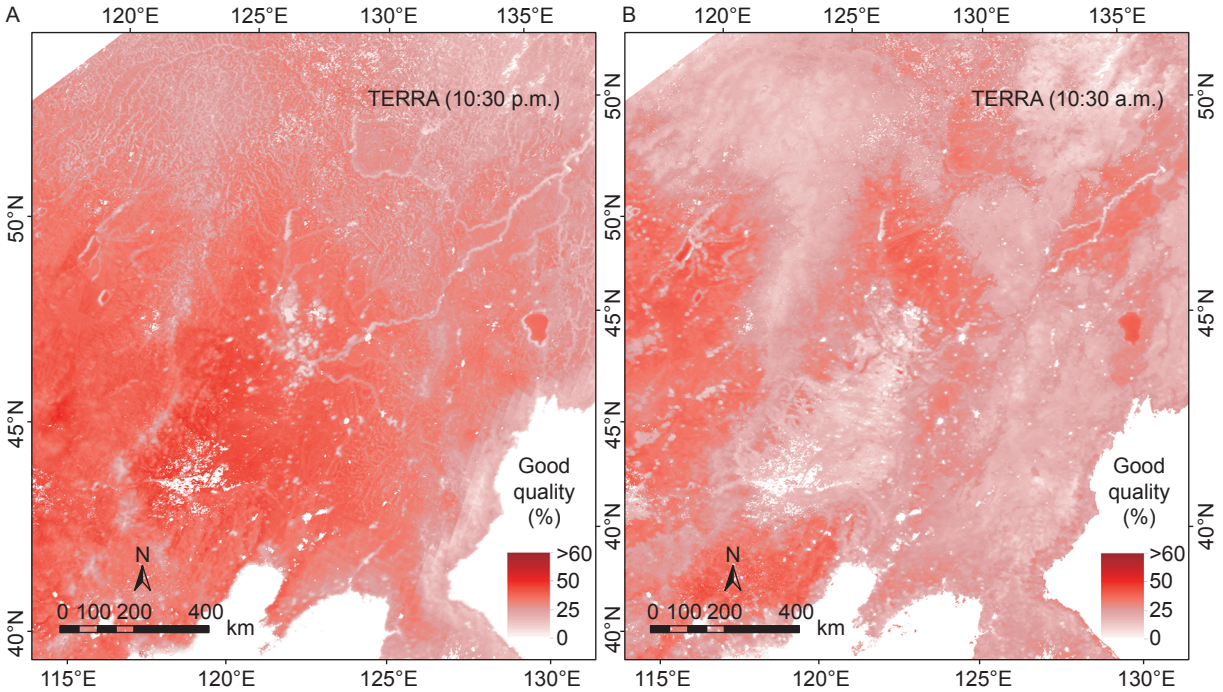

Fig. 3 Percentage of good quality TERRA land surface temperature pixels from 2003 to 2015.

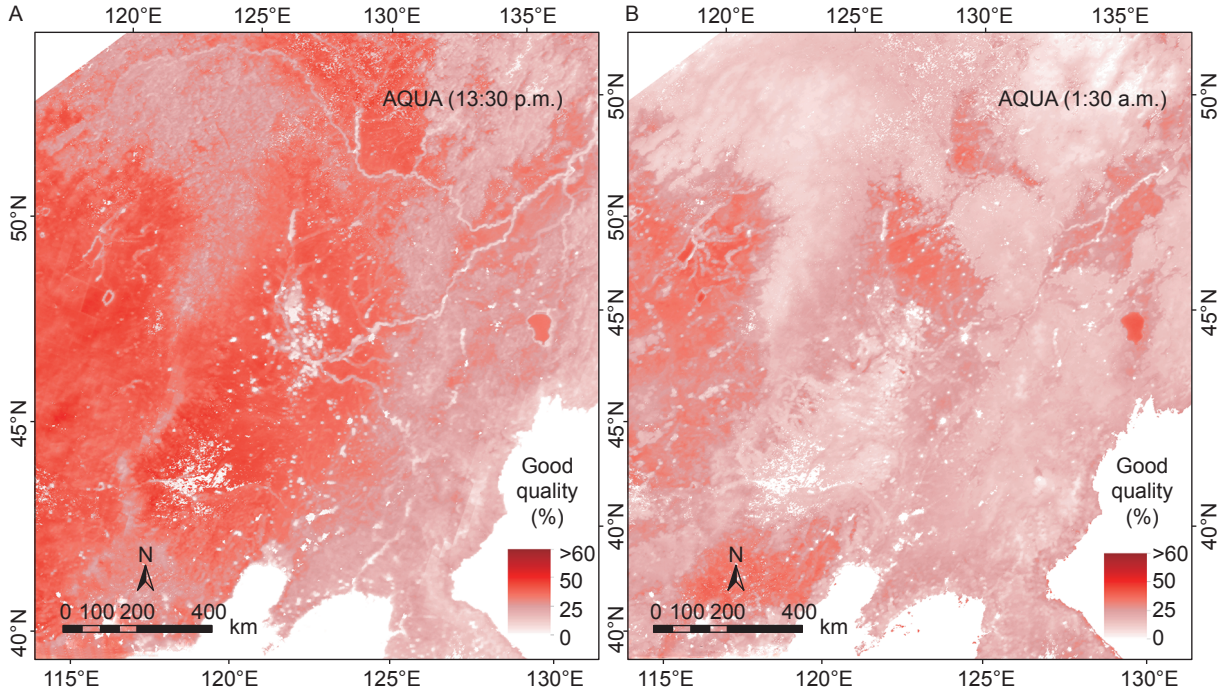

Fig. 4 Percentage of good quality AQUA land surface temperature pixels from 2003 to 2015.

soil temperature. Therefore, precipitation and soil water content can affect the spatial relationship between soil temperature and LST, and this has a potential to influence soil temperature estimation accuracy when satellite data are involved.

5. Conclusion

In this paper, regional soil temperatures at depths ranging from 0 to 40 cm down the soil profile are estimated using linear regression models based on LST and NDVI obtained from MODIS AQUA and TERRA products together with ancillary Ds data. The proposed models are validated against *in-situ* measurements obtained from meteorological stations at a test site located in northern China.

Our results show that LST and NDVI values derived from MODIS AQUA and TERRA, and Ds, are good predictors of soil temperatures. Multiple linear regression models involving predictor variables from MODIS products have been proposed to be suitable in this paper. With the maximum R^2 and the minimum RMSE being recorded at depths of 5 cm or 10 cm, MODIS data can be regarded effective in estimating soil temperatures in the humus layer of the soil profile where microbial activities are most prominent, and where shallow-rooted crops such as cereals and grain legumes are confined. This application would provide data of relevance to cropping calendars as selection of suitable planting time is related to soil temperature.

In view of the relatively poor performance of the estimation models used in this study at depths greater than 15 cm, the use of more advanced regression models such as those based on support vector machine, artificial neural network, Random Forest and adaptive-network-based fuzzy inference system which are capable of learning from data rather than relying on apparent linear correlations, could optimize the relationship between predictor and response variables to achieve a soil temperature estimation accuracy that can fulfill the requirements of precision agricultural initiatives.

Acknowledgements

This study was supported by the National Natural Science Foundation of China (41671418 and 41371326), the Science and Technology Facilities Council of UK-Newton Agritech Programme (Sentinels of Wheat), and the Fundamental Research Funds for the Central Universities, China (2019TC117).

References

Agnew M D, Palutikof J P. 2000. GIS-based construction of baseline climatologies for the Mediterranean using terrain variables. *Climate Research*, **14**, 115–127.

Araghi A, Mousavi-Baygi M, Adamowski J. 2017. Detecting soil temperature trends in Northeast Iran from 1993 to 2016.

Soil & Tillage Research, **174**, 177–192.

Barringer J R F. 1997. Meso-scale mapping of soil temperatures in the mackenzie basin, New Zealand. In: *Annual Conference of GeoComputation*. University of Otago, New Zealand.

Beck C B. 2010. *An Introduction to Plant Structure and Development*: *Preface to the Second Edition*. Cambridge University Press, Cambridge.

Bourges B. 1985. Improvement in solar declination computation. *Solar Energy*, **35**, 367–369.

Burrough P A. 1986. Principles of geographical information systems for land resource assessment. *Landscape & Urban Planning*, **15**, 357–358.

Bustos E, Meza F J. 2015. A method to estimate maximum and minimum air temperature using MODIS surface temperature and vegetation data: Application to the Maipo Basin, Chile. *Theoretical and Applied Climatology*, **120**, 211–226.

Cai Y L, Chen G, Wang Y L, Yang L. 2017. Impacts of land cover and seasonal variation on maximum air temperature estimation using MODIS imagery. *Remote Sensing*, **9**, 233.

Casey K A, Polashenski C M, Chen J, Tedesco M. 2017. Impact of MODIS sensor calibration updates on Greenland Ice Sheet surface reflectance and albedo trends. *Cryosphere*, **11**, 1781–1795.

Chen J, Jönsson P, Tamura M, Gu Z H, Matsushita B, Eklundhd L. 2004. A simple method for reconstructing a high-quality NDVI time-series data set based on the Savitzky-Golay filter. *Remote Sensing of Environment*, **91**, 332–344.

Chen S S, Chen X Z, Chen W Q, Su Y X, Li D. 2011. Error sources in remote sensing of microwave land surface emissivity. *International Journal of Applied Earth Observation and Geoinformation*, **13**, 140–151.

Colliander A, Fisher J B, Halverson G, Merlin O, Misra S, Bindlish R, Jackson T J, Yueh S. 2017. Spatial downscaling of SMAP soil moisture using MODIS land surface temperature and NDVI during SMAPVEX15. *IEEE Geoscience and Remote Sensing Letters*, **14**, 2107–2111.

Daly C. 2006. Guidelines for assessing the suitability of spatial climate data sets. *International Journal of Climatology*, **26**, 707–721.

Didari S, Norouzi H, Zand-Parsa S, Khanbilvardi R. 2017. Estimation of daily minimum land surface air temperature using modis data in southern iran. *Theoretical and Applied Climatology*, **130**, 1149–1161.

Duguay-Tetzlaff A, Bento V A, Göttsche F M, Stöckli R, Martins J P A, Trigo I, Olesen F, Bojanowski J S, Da Camara C, Kunz H. 2015. Meteosat land surface temperature climate data record: Achievable accuracy and potential uncertainties. *Remote Sensing*, **7**, 13139–13156.

Du L T, Song N P, Liu K, Hou J. 2017. Comparison of two simulation methods of the temperature vegetation dryness index (TVDI) for drought monitoring in semi-arid regions of China. *Remote Sensing*, **9**, 177.

Fangueiro D, Kidd P S, Alvarenga P, Beesley L, de Varennes A. 2018. Strategies for soil protection and remediation. In: Duarte A C, Cachada A, Rocha-Santos T, eds., *Soil Pollution*. Academic Press, USA. pp. 251–281.

Feng X M, Cai DL. 2004. Soil temperature in relation to air temperature, altitude and latitude. *Acta Pedologica Sinica*, **41**, 489–491. (in Chinese)

Fily M, Royer A, Goïta K, Prigent C. 2003. A simple retrieval method for land surface temperature and fraction of water surface determination from satellite microwave brightness temperatures in sub-arctic areas. *Remote Sensing of Environment*, **85**, 328–338.

Freitas S C, Trigo I F, Bioucas-Dias J M, Gottsche FM. 2010. Quantifying the uncertainty of land surface temperature retrievals from SEVIRI/Meteosat. *IEEE Transactions on Geoscience and Remote Sensing*, **48**, 523–534.

Friedl M A, McIver D K, Hodges J C, Zhang X Y, Muchoney D, Strahler A H, Woodcock C E, Gopal S, Schneider A, Cooper A, Baccini A, Gao F, Schaaf C. 2002. Global land cover mapping from MODIS: Algorithms and early results. *Remote Sensing of Environment*, **83**, 287–302.

Gao H L, Fu R, Dickinson R E, Juarez R I N. 2008. A practical method for retrieving land surface temperature from AMSR-E over the Amazon Forest. *IEEE Transactions on Geoscience and Remote Sensing*, **46**, 193–199.

Gao Z Q, Gao W, Chang N B. 2011. Integrating temperature vegetation dryness index (TVDI) and regional water stress index (RWSI) for drought assessment with the aid of LANDSAT TM/ETM plus images. *International Journal of Applied Earth Observation and Geoinformation*, **13**, 495–503.

Gasch C K, Hengl T, Graler B, Meyer H, Magney T S, Browna D J. 2015. Spatio-temporal interpolation of soil water, temperature, and electrical conductivity in 3D+T: The Cook Agronomy Farm data set. *Spatial Statistics*, **14**, 70–90.

Göttsche F M, Olesen F S. 2001. Land surface temperature retrieval from MSG1-SEVIRI data. *Remote Sensing of Environment*, **76**, 337–348.

Göttsche F M, Olesen F S, Bork-Unkelbach A. 2013. Validation of land surface temperature derived from MSG/SEVIRI with *in situ* measurements at Gobabeb, Namibia. *International Journal of Remote Sensing*, **34**, 3069–3083.

Gaur A, Eichenbaum M K, Simonovic S P. 2018. Analysis and modelling of surface Urban Heat Island in 20 Canadian cities under climate and land-cover change. *Journal of Environmental Management*, **206**, 145–157.

Guillevic P C, Privette J L, Coudert B, Palecki M A, Demarty J, Ottlé C, Augustine J A. 2012. Land surface temperature product validation using NOAA's surface climate observation networks — Scaling methodology for the Visible Infrared Imager Radiometer Suite (VIIRS). *Remote Sensing of Environment*, **124**, 282–298.

Guillevic P C, Biard J C, Hulley G C, Privette J L, Hook S J, Olioso A, Göttsche F M, Radocinski R, Román M O, Yu Y Y, Csiszar I. 2014. Validation of Land Surface Temperature products derived from the Visible Infrared Imaging Radiometer Suite (VIIRS) using ground-based and heritage satellite measurements. *Remote Sensing of Environment*, **154**, 19–37.

He Z H, Zeng Z C, Lei L P, Bie N. 2017. A Data-Driven Assessment of biosphere-atmosphere interaction impact on seasonal cycle patterns of XCO_2 using GOSAT and MODIS observations. *Remote Sensing*, **9**, 251.

Hillel D. 1998. *Environmental Soil Physics*. Academic Press, USA. pp. 309–334.

Hu Q, Feng S. 2003. A daily soil temperature dataset and soil temperature climatology of the contiguous United States. *Journal of Applied Meteorology*, **42**, 1139–1156.

Huang C L, Li X, Lu L. 2008. Retrieving soil temperature profile by assimilating MODIS LST products with ensemble Kalman filter. *Remote Sensing of Environment*, **112**, 1320–1336.

Huang J X, Gomez-Dans J, Huang H, Ma H Y, Wu Q L, Lewis E P, Liang S L, Chen Z X, Xue J H, Wu Y T, Zhao F, Wang J, Xie X H. 2019a. Assimilation of remote sensing into crop growth models: Current status and perspectives. *Agricultural and Forest Meteorology*, **276**, 276–277.

Huang J X, Ma H Y, Sedano F, Lewis P, Liang, S L, Wu Q L, Su W, Zhang X D, Zhu D H. 2019b. Evaluation of regional estimates of winter wheat yield by assimilating three remotely sensed reflectance datasets into the coupled WOFOST–PROSAIL model. *European Journal of Agronomy*, **102**, 1–13.

Huang J X, Sedano F, Huang Y B, Ma H Y, Liu X L, Liang S L, Tian L Y, Zhang X D, Fan J L, Wu W B. 2016. Assimilating a synthetic Kalman filter leaf area index series into the WOFOST model to improve regional winter wheat yield estimation. *Agricultural and Forest Meteorology*, **216**, 188–202.

Huang J X, Tian L Y, Liang S L, Ma H Y, Becker-Reshef I, Huang Y B, Su W, Zhang X D, Zhu D H, Wu W B. 2015. Improving winter wheat yield estimation by assimilation of the leaf area index from Landsat tm and MODIS data into the WOFOST model. *Agricultural and Forest Meteorology*, **204**, 106–121.

Huang J X, Wang H M, Dai Q, Han D W. 2014. Analysis of NDVI data for crop identification and yield estimation. *IEEE Journal of Selected Topics in Applied Earth Observations and Remote Sensing* **7**, 4374–4384.

Huang J X, Wu S, Liu X, Ma G N. 2012. Regional winter wheat yield forecasting based on assimilation of remote sensing data and crop growth model with ensemble Kalman method. *Transactions of the Chinese Society of Agricultural Engineering*, **28**, 142–148.

Huang R, Zhang C, Huang J X, Zhu D H, Wang L M, Liu J. 2015. Mapping of daily mean air temperature in agricultural regions using daytime and nighttime land surface temperatures derived from TERRA and AQUA MODIS data. *Remote Sensing*, **7**, 8728–8756.

Huang W J, Li J, Guo Q Y, Mansaray L R, Li X X, Huang J F. 2017. A satellite-derived climatological analysis of urban heat island over Shanghai during 2000–2013. *Remote Sensing*, **9**, 641.

Huang Y B, Chen Z X, Tao Y, Huang X Z, Gu X F. 2018. Agricultural remote sensing big data: Management and applications. *Journal of Integrative Agriculture*, **9**, 1915–1931.

Islam T, Hulley G C, Malakar N K, Radocinski R G, Guillevic P C, Hook S J. 2017. A physics-based algorithm for the simultaneous retrieval of land surface temperature and emissivity from VIIRS thermal infrared data. *IEEE Transactions on Geoscience and Remote Sensing*, **55**, 563–576.

Jebamalar A S, Raja S A T, Bai S J S. 2012. Prediction of annual and seasonal soil temperature variation using artificial neural network. *Indian Journal of Radio and Space Physics*, **41**, 48–57.

Jiang G M, Liu R G. 2015. Retrieval of sea and land surface temperature from SVISSR/FY-2C/D/E measurements. *IEEE Transactions on Geoscience and Remote Sensing*, **52**, 6132–6140.

Jiang J, Li H, Liu Q, Wang H, Du Y, Cao B, Zhong B, Wu S. 2015. Evaluation of land surface temperature retrieval from FY-3B/VIRR Data in an arid area of northwestern China. *Remote Sensing*, **7**, 7080–7104.

Jin M S, Mullens T. 2014. A Study of the relations between soil moisture, soil temperatures and surface temperatures using ARM observations and offline CLM4 simulations. *Climate*, **2**, 279–295.

Kang S, Kim S, Oh S, Lee D. 2000. Predicting spatial and temporal patterns of soil temperature based on topography, surface cover and air temperature. *Forest Ecology and Management Forest*, **136**, 173–184.

Kou X, Jiang L, Bo Y, Yan S, Chai L. 2016. Estimation of land surface temperature through blending MODIS and AMSR-E data with the bayesian maximum entropy method. *Remote Sensing*, **8**, 105.

Lehnert M. 2013. The soil temperature regime in the urban and suburban landscapes of olomouc, czech republic. *Moravian Geographical Reports*, **21**, 27–36.

Li H, Sun D L, Yu Y Y, Wang H Y, Liu Y L, Liu Q H, Du Y M, Wang H S, Cao B. 2014. Evaluation of the VIIRS and MODIS LST products in an arid area of Northwest China. *Remote Sensing of Environment*, **142**, 111–121.

Liao C H, Wang J F, Pritchard I, Liu J G, Shang J L. 2017. A spatio-temporal data fusion model for generating NDVI time series in heterogeneous regions. *Remote Sensing*, **9**, 1125.

Lin S P, Moore N J, Messina J P, DeVisser M H, Wu J P. 2012. Evaluation of estimating daily maximum and minimum air temperature with MODIS data in east Africa. *International Journal of Applied Earth Observation and Geoinformation*, **18**, 128–140.

Liu Y, Yu Y, Yu P, Göttsche F M, Trigo I F. 2015. Quality assessment of S-NPP VIIRS land surface temperature product. *Remote Sensing*, **7**, 12215–12241.

Liu Z H, Wu P H, Duan S B, Zhan W F, Ma X S, Wu Y L. 2017. Spatiotemporal reconstruction of land surface temperature derived from fengyun geostationary satellite data. *IEEE Journal of Selected Topics in Applied Earth Observations and Remote Sensing*, **10**, 4531–4543.

Mackiewicz M C. 2012. A new approach to quantifying soil temperature responses to changing air temperature and snow cover. *Polar Science*, **6**, 226–236.

Mechri R, Ottlé C, Pannekoucke O, Kallel A, Maignan F, Courault D, Trigo I F. 2016. Downscaling meteosat land surface temperature over a heterogeneous landscape using a data assimilation approach. *Remote Sensing*, **8**, 586.

Meng Q Y, Zhang L L, Sun Z H, Meng F, Wang L, Sun Y X. 2018. Characterizing spatial and temporal trends of surface urban heat island effect in an urban main built-up area: A 12-year case study in Beijing, China. *Remote Sensing of Environment*, **204**, 826–837.

Mitasova H, Mitas L. 2001. Multiscale soil erosion simulations for land use management. In: Harmon R S, Doell W W, eds., *Landscape Erosion and Evolution Modeling*. Springer, Boston. pp. 321–347.

Moran M S, Scott R L, Keefer T O. Nearing G S, Paige G B, Cosh M H, O'Neill P E. 2009. Partitioning evapotranspiration in semiarid grassland and shrubland ecosystems using time series of soil surface temperature. *Agricultural and Forest Meteorology*, **149**, 59–72.

Niclòs R, Pérez-Planells L, Coll C, Valiente J A, Valor E. 2018. Evaluation of the S-NPP VIIRS land surface temperature product using ground data acquired by an autonomous system at a rice paddy. *Journal of Photogrammetry and Remote Sensing*, **135**, 1–12.

Peon J, Recondo C, Calleja J F. 2014. Improvements in the estimation of daily minimum air temperature in peninsular Spain using MODIS land surface temperature. *International Journal of Remote Sensing*, **35**, 5148–5166.

Peng D L, Huete A R, Huang J F, Wang F M, Sun H S. 2011. Detection and estimation of mixed paddy rice cropping patterns with MODIS data. *International Journal of Applied Earth Observation and Geoinformation*, **13**, 13–23.

Petrou Z I, Tian Y L. 2017. High-resolution sea ice motion estimation with optical flow using satellite spectroradiometer data. *IEEE Transactions on Geoscience and Remote Sensing*, **55**, 1339–1350.

Prigent C, Jimenez C, Aires F. 2016. Toward "all weather," long record, and real-time land surface temperature retrievals from microwave satellite observations. *Journal of Geophysical Research* (Atmospheres), **121**, 5699–5717.

Rasmussen M O, Gottsche F M, Olesen F S, Sandholt I. 2011. Directional effects on land surface temperature estimation from meteosat second generation for savanna landscapes. *IEEE Transactions on Geoscience and Remote Sensing*, **49**, 4458–4468.

Savitzky A, Golay M J E. 1964. Smoothing and differentiation of data by simplified least squares procedures. *Analytical Chemistry*, **36**, 1627–1639.

Skakun S, Franch B, Vermote E, Roger J, Becker-Reshef I, Justice C, Kussul N. 2017. Early season large-area winter crop mapping using MODIS NDVI data, growing degree days information and a Gaussian mixture model. *Remote Sensing of Environment*, **195**, 244–258.

Shati F, Prakash S, Norouzi H, Blake R. 2018. Assessment of differences between near-surface air and soil temperatures for reliable detection of high-latitude freeze and thaw states. *Cold Regions Science and Technology*, **145**, 86–92.

Sobrino J A, Romaguera M. 2004. Land surface temperature retrieval from MSG1-SEVIRI data. *Remote Sensing of Environment*, **92**, 247–254.

Song C Y, Jia L, Menenti M. 2014. Retrieving high-resolution surface soil moisture by downscaling AMSR-E brightness temperature using MODIS LST and NDVI data. *IEEE Journal of Selected Topics in Applied Earth Observations and Remote Sensing*, **7**, 935–942.

Song X N, Wang Y W, Tang B H, Leng P, Chuan S, Peng J, Loew A. 2017. Estimation of land surface temperature using feng yun-2E (FY-2E) data: A case study of the source area of the yellow river. *IEEE Journal of Selected Topics in Applied Earth Observations and Remote Sensing*, **10**, 3744–3751.

Tabbagh A, Guérin R, Cheviron B, Henine H. 2016. Seasonal monitoring of soil water content and infiltration using soil temperature measurements. In: *Proceedings of the Near Surface Geoscience*, 22nd European Meeting of Environmental and Engineering Geophysics, Barcelona, Spain.

Tang B H, Bi Y Y, Li Z L, Xia J. 2008. Generalized Split-window algorithm for estimate of land surface temperature from chinese geostationary fengyun meteorological satellite (FY-2C) data. *Sensors*, **8**, 933–951.

Tang B H, Shao K, Li Z L, Wu H, Nerry F, Zhou G. 2015. Estimation and validation of land surface temperatures from chinese second-generation polar-orbit FY-3A VIRR data. *Remote Sensing*, **7**, 3250–3273.

Tong X Y, Brandt M, Hiernaux P, Herrmann S M, Tian F, Prishchepov A V, Fensholt R. 2017. Revisiting the coupling between NDVI trends and cropland changes in the Sahel drylands: A case study in western Niger. *Remote Sensing of Environment*, **191**, 286–296.

Vicente-Serrano S M, Saz-Sanchez M A, Cuadrat J M. 2003. Comparative analysis of interpolation methods in the middle Ebro Valley (Spain): Application to annual precipitation and temperature. *Climate Research*, **24**, 161–180.

Wan Z M, Dozier J. 1996. A generalized split-window algorithm for retrieving land-surface temperature from space. *IEEE Transactions on Geoscience and Remote Sensing*, **34**, 892–905.

Wang X X, Luo G P, Hui Y, Zhang Q, Cai P, Zhang M. 2017. Construction of mean air temperature datasets with high temporal and spatial resolution in oasis-desert region: A case study of Sangong river basin on the northern slope of Tianshan Mountains. *Geographical Research*, **36**, 49–60. (in Chinese)

Webster R, Oliver M A. 1992. Sample adequately to estimate variograms of soil properties. *European Journal of Soil Science*, **43**, 177–192.

Wu P H, Shen H F, Zhang L P, Göttsche F M. 2015. Integrated fusion of multi-scale polar-orbiting and geostationary satellite observations for the mapping of high spatial and temporal resolution land surface temperature. *Remote Sensing of Environment*, **156**, 169–181.

Wu W, Tang X P, Guo N J, Yang C, Liu H B, Shang Y F. 2013.

Spatiotemporal modeling of monthly soil temperature using artificial neural networks. *Theoretical and Applied Climatology*, **113**, 481–494.

Wu W, Tang X P, Ma X Q, Liu H B. 2016. A comparison of spatial interpolation methods for soil temperature over a complex topographical region. *Theoretical and Applied Climatology*, **125**, 657–667.

Yang H, Weng F Z. 2011. Error sources in remote sensing of microwave land surface emissivity. *IEEE Transactions on Geoscience and Remote Sensing*, **49**, 3437–3442.

Yang X M. 1989. Soil hydrothermal conditions and soil system classification. *Soils*, **2**, 56–59. (in Chinese)

Yoo C, Im J, Park S, Quackenbush L J. 2018. Estimation of daily maximum and minimum air temperatures in urban landscapes using MODIS time series satellite data. *Journal of Photogrammetry and Remote Sensing*, **137**,149–162.

Yu Y Y, Privette J L, Pinheiro A C. 2005. Analysis of the NPOESS VIIRS land surface temperature algorithm using MODIS data. *IEEE Transactions on Geoscience and Remote Sensing*, **43**, 2340–2350.

Zhang D, Hunt E R, Running S W. 1993. A daily soil temperature model based on air temperature and precipitation for continental applications. *Climate Research*, **2**, 183–191.

Zhang H B, Zhang F, Ye M, Che T, Zhang G Q. 2016. Estimating daily air temperatures over the Tibetan Plateau by dynamically integrating MODIS LST data. *Journal of Geophysical Research-Atmospheres*, **121**, 11425–11441.

Zhang X L, Wu S, Yan X D, Chen Z J. 2017. A global classification of vegetation based on NDVI, rainfall and temperature. *International Journal of Climatology*, **37**, 2318–2324.

Zhou F C, Li Z L, Wu H, Duan S B, Song X N, Yan G J. 2018. A practical two-stage algorithm for retrieving land surface temperature from AMSR-E data — a case study over China. *IEEE Journal of Selected Topics in Applied Earth Observations and Remote Sensing*, **11**, 1939–1948.

Zhou J, Zhang X D, Zhan W F, Göttsche FM, Liu S, Olesen F S, Hu W X, Dai F N. 2017. A thermal sampling depth correction method for land surface temperature estimation from satellite passive microwave observation over barren land. *IEEE Transactions on Geoscience and Remote Sensing*, **55**, 4743–4756.

Zhuo W, Huang J X, Li L, Zhang X D, Ma H Y, Gao X R, Huang H, Xu B D, Xiao X M. 2019. Assimilating soil moisture retrieved from Sentinel-1 and Sentinel-2 data into WOFOST model to improve winter wheat yield estimation. *Remote Sensing*, **11**, 1618–1634.

Executive Editor-in-Chief ZHANG Wei-li
Managing editor SUN Lu-juan